



CrossMark  
click for updates

Cite this: *RSC Adv.*, 2016, 6, 9857

# Discovery of neuroprotective compounds by machine learning approaches†

Jiansong Fang,<sup>‡ab</sup> Xiaocong Pang,<sup>‡a</sup> Rong Yan,<sup>a</sup> Wenwen Lian,<sup>a</sup> Chao Li,<sup>a</sup> Qi Wang,<sup>b</sup> Ai-Lin Liu<sup>\*acd</sup> and Guan-Hua Du<sup>\*acd</sup>

Neuronal cell death from oxidative stress is a strong factor of many neurodegenerative diseases. To tackle these problems, phenotypic drug screening assays are a possible alternative strategy. The aim of this study is to develop the neuroprotective models against glutamate or H<sub>2</sub>O<sub>2</sub>-induced neurotoxicity by machine learning approaches, which helps in discovering neuroprotective compounds. Four different single classifiers (neural network, *k* nearest neighbors, classification tree and random forest) were constructed based on two large datasets containing 1260 and 900 known active or inactive compounds, which were integrated to develop the combined Bayesian models to obtain superior performance. Our results showed that both of the Bayesian models (combined-NB-1 and combined-NB-2) outperformed the corresponding four single classifiers. Additionally, structural fingerprint descriptors were added to improve the predictive ability of the models, resulting in the two best models NB-1-LPFP4 and NB-2-LCFP6. The best two models gave Matthews correlation coefficients of 0.972 and 0.956 for 5-fold cross validation as well as 0.953 and 0.902 for the test set, respectively. To illustrate the practical applications of the two models, NB-1-LPFP4 and NB-2-LCFP6 were used to perform virtual screening for discovering neuroprotective compounds, and 70 compounds were selected for further cell-based assay. The assay results showed that 28 compounds exhibited neuroprotective effects against glutamate-induced and H<sub>2</sub>O<sub>2</sub>-induced neurotoxicity simultaneously. Our results suggested the method that integrated single classifiers into combined Bayesian models could be feasible to predict neuroprotective compounds.

Received 2nd November 2015  
Accepted 14th January 2016

DOI: 10.1039/c5ra23035g

www.rsc.org/advances

<sup>a</sup>Institute of Materia Medica, Chinese Academy of Medical Sciences and Peking Union Medical College, 1 Xian Nong Tan Street, Beijing 100050, PR China. E-mail: liualin@imm.ac.cn; dugh@imm.ac.cn; Fax: +86-10-83150885; +86-10-63165184; Tel: +86-10-83150885; +86-10-63165184

<sup>b</sup>Institute of Clinical Pharmacology, Guangzhou University of Traditional Chinese Medicine, Guangzhou 510006, China

<sup>c</sup>Beijing Key Laboratory of Drug Target and Screening Research, Beijing 100050, PR China

<sup>d</sup>State Key Laboratory of Bioactive Substance and Function of Natural Medicines, Beijing 100050, PR China

† Electronic supplementary information (ESI) available: Y-scrambling result of NB-1-LPFP4 and NB-2-LCFP6 (Fig. S1), extracting applicability domain for a QSAR model-step by step (Fig. S2), the structures (in SMILE format) of the 1000 compounds of the training set and 260 compounds of the test set for glutamate-induced models (Tables S1–S2), the structures (in SMILE format) of the 700 compounds of the training set and 200 compounds of the test set for H<sub>2</sub>O<sub>2</sub>-induced models (Tables S3–S4), the detailed performance of 24 single classification models for 5-fold cross validation and test set using different combinational of molecular properties (Table S5), the detailed performance of the 26 combined Bayesian classification models for 5-fold cross validation and test set using different combinational of output probabilities and fingerprints (Table S6), and the structures (in SMILE format) (Table S7) and preliminary assay result (Table S8) for 70 virtual hits on monosodium glutamate or H<sub>2</sub>O<sub>2</sub>-induced neurotoxicity on PC12 Cell. See DOI: 10.1039/c5ra23035g

‡ These authors contributed equally.

## 1 Introduction

Neurodegenerative disease is an umbrella term characterized by progressive loss of structure or function of neurons, which includes Alzheimer's, Parkinson's, and Huntington's disease.<sup>1</sup> Oxidative stress caused by excessive reactive oxygen species (ROS) production is a common culprit of many neurodegenerative diseases.<sup>2,3</sup>

The most common ROS are oxygen radicals, such as superoxide and hydroxyl radicals, and non-free radicals, such as hydrogen peroxide (H<sub>2</sub>O<sub>2</sub>). H<sub>2</sub>O<sub>2</sub>, the main form of ROS, is produced during the redox process and is recognized as a messenger in intracellular signaling cascades.<sup>4</sup> In addition, H<sub>2</sub>O<sub>2</sub> can cause oxidative damage to molecules such as carbohydrates, proteins, lipids, and DNA, and at last cell death.<sup>5</sup> Besides, elevated levels of the excitatory amino acid glutamate can also lead to oxidative stress-dependent neuronal death. Glutamate is considered as the major excitatory neurotransmitter in the central nervous system (CNS), and glutamate-induced excitotoxicity is known to be a major contributor to pathological cell death within the nervous system.<sup>6</sup> Consequently, the searching for effective treatments that prevent oxidative stress associated with neurodegenerative diseases is an issue of crucial importance.



parts were processed by the addition of hydrogen atoms, the deprotonation of strong acids, the protonation of strong bases, the generation of valid three-dimensional conformation through washing, and the minimization of energy using the software of Molecular Operating Environment (MOE).<sup>27</sup> All active compounds are labelled as “1”, while decoys exhibiting no neuroprotective activity were labelled as “0”.

## 2.2 Molecular descriptors

Each compound was represented with three sets of two-dimensional (2D) descriptors using Discovery Studio 4.0 (DS 4.0)<sup>28</sup> and MOE 2010 software.<sup>27</sup> The first set of descriptors including 256 2D descriptors was calculated by DS 4.0, which were made up of AlogP, estate keys, molecular properties, molecular property counts, surface area and volume, and topological descriptors. MOE 2010 was another software used to calculate the second set of descriptors containing 185 2D descriptors. The last set of descriptors were composed of the first two sets of descriptors, which consisted of 441 (256+185) descriptors.

Molecular fingerprints in this paper were also calculated with DS 4.0, including the SciTegic extended-connectivity fingerprints (FCFP and ECFP) and Daylight-style path-based fingerprints (FPFP and EPFP). The fingerprints used here are different from the substructures in a binary form. They stand for a much larger set of features than predefined substructures. Besides, they do not need to be preselected or predefined because they can be generated directly from the molecules. Given that the structural fragments should neither be too small nor too large, two diameters, 4 and 6, were chosen for each fingerprint.

## 2.3 Molecular descriptor selection

Pearson correlation analysis<sup>29</sup> can eliminate molecular descriptors that are not significantly correlated with activity and highly correlated with each other. In this study, the descriptors exhibiting a Pearson correlation coefficient ( $P < 0.1$ ) with the activity were removed. If the pairwise correlation coefficient between any two descriptors was higher than 0.9, the descriptor which had a lower correlation coefficient with the activity would be deleted. After that, genetic search in Weka 3.6 was carried out to further eliminate the descriptors.<sup>30</sup> Genetic algorithms are search algorithms based on the mechanics of natural selection and natural genetics,<sup>31</sup> while Weka is a collection of machine learning algorithms for data mining, including a number of methods for data preprocessing, attribute selection, classification, etc. Finally, the descriptors chosen from different sets of descriptors are listed in Table 2.

## 2.4 Methods for model building

Five different machine learning tools, including neural network (NN),  $k$  nearest neighbors ( $k$ NN), classification tree (CT), random forest (RF) and naive Bayesian (NB), were employed with the entire computational workflow. NN,  $k$ NN, CT and RF were performed in Orange canvas 2.7.<sup>32</sup> NB was performed using DS 4.0. In this paper, all models developed get two probability output (positive and negative probability) as well as estimated target values (such as 1 or 0).

### 2.4.1 Single classifier model

**2.4.1.1 Neural network (NN).** NN is an information processing paradigm that is inspired by the way biological nervous systems, such as the brain, process information.<sup>33</sup> In Orange canvas 2.7, neural network learner implements a multilayer perceptron. Learning is performed by minimizing an L2-regularized cost function with scipy's implementation of L-BFGS. The value of hidden layer neurons, regularization factor, and max iterations was set to 20, 1.0 and 300, respectively.

**2.4.1.2  $k$  nearest neighbors ( $k$ NN).** The  $k$ NN algorithm is an algorithm to classify objects based on closest examples in the feature space.<sup>34</sup> An object is classified by a majority vote of its neighbors, with the object being assigned to the class most common among its  $k$  nearest neighbors ( $k$  is a positive integer). In this paper, the nearness is measured by Euclidean distance metrics and the number of neighbors ( $k$ ) was set to 5.

**2.4.1.3 Classification tree (CT).** In classification tree, leaves stand for class labels and branches represent conjunctions of features that lead to those class labels. Orange includes multiple implementations of classification tree learners. In this study, the C4.5 tree induction algorithm was implemented. C4.5 is an algorithm used to generate a decision tree developed by Ross Quinlan,<sup>35</sup> which builds decision trees from a set of training data by means of a hill-climbing search based on the statistical property measure called information gain. The parameters here were adopted with the default setting.

**2.4.1.4 Random forest (RF).** RF is a classification technique that operates by constructing a multitude of decision trees at training time and outputting the class that is the mode of the classes output by individual trees. Each tree is built from a bootstrap sample from the training data. When developing individual trees, an arbitrary subset of attributes is drawn (called “random”) from which the best attribute for the split is selected. The classification is based on the majority vote from individually developed tree classifiers in the forest. A detailed descriptions of RF can be found in the original literature.<sup>36</sup> In this work, the number of trees in forest was set to 10, while nodes were stopped splitting with 5 or fewer instances.

Table 1 Detailed statistical description of the entire data set

| Model                                  | Training set (ECFP2) |        |       |                | Test set (ECFP2) |        |       |                |
|----------------------------------------|----------------------|--------|-------|----------------|------------------|--------|-------|----------------|
|                                        | Inhibitors           | decoys | Total | Tanimoto index | Inhibitors       | decoys | Total | Tanimoto index |
| Glutamate-induced                      | 200                  | 800    | 1000  | 0.125          | 52               | 208    | 260   | 0.132          |
| H <sub>2</sub> O <sub>2</sub> -induced | 140                  | 560    | 700   | 0.142          | 40               | 160    | 200   | 0.162          |

Table 2 Molecular descriptors used in this work<sup>a</sup>

| No.            | Descriptor class | Number of descriptors | Descriptors                                                                                                                                                                                                                                                                                                         |
|----------------|------------------|-----------------------|---------------------------------------------------------------------------------------------------------------------------------------------------------------------------------------------------------------------------------------------------------------------------------------------------------------------|
| 1 <sup>#</sup> | DS 2D            | 12                    | ES_Count_aasC, ES_Sum_dO, ES_Sum_ssCH2, SAScore_Complexity, HBD_Count, Num_AliphaticSingleBonds, Num_DoubleBonds, Num_RingBonds, Num_Rings6, CIC, IAC_Mean, SC_3_C                                                                                                                                                  |
| 2 <sup>#</sup> | MOE 2D           | 21                    | a_don, a_ICM, balabanJ, BCUT_SMR_1, chi1_C, density, GCUT_SLOGP_1, GCUT_SLOGP_2, PEOE_RPC+, PEOE_VSA4+, PEOE_VSA0, PEOE_VSA2, PEOE_VSA3, PEOE_VSA4, PEOE_VSA5, PEOE_VSA_POL, PEOE_VSA_POS, PEOE_VSA_PPOS, SlogP_VSA4, SlogP_VSA5, SMR_VSA1, SMR_VSA5, SMR_VSA6                                                      |
| 3 <sup>#</sup> | DS 2D and MOE 2D | 26                    | ES_Sum_ssCH2, SAScore_Complexity, Num_Rings6, CIC, IAC_Mean, a_don, balabanJ, BCUT_SMR_1, chi1_C, density, GCUT_SLOGP_1, GCUT_SLOGP_2, PEOE_RPC+, PEOE_VSA4+, PEOE_VSA_0, PEOE_VSA_2, PEOE_VSA_3, PEOE_VSA_4, PEOE_VSA_5, PEOE_VSA_POL, PEOE_VSA_POS, PEOE_VSA_PPOS, SlogP_VSA4, SlogP_VSA5, SMR_VSA1, SMR_VSA6     |
| 4 <sup>#</sup> | DS 2D            | 12                    | ES_Count_aasC, ES_Count_dssC, ES_Count_ssCH2, ES_Sum_ssCH2, QED_HBD, SAScore_Complexity, HBD_Count, Num_AtomClasses, Num_H_Acceptors, Num_Rings5, IAC_Mean, SC_3_C                                                                                                                                                  |
| 5 <sup>#</sup> | MOE 2D           | 26                    | a_acc, a_nN, BCUT_PEOE_0, BCUT_SLOGP_1, GCUT_SLOGP_0, GCUT_SLOGP_2, GCUT_SMR_1, opr_brigid, PEOE_VSA+2, PEOE_VSA+3, PEOE_VSA+4, PEOE_VSA0, PEOE_VSA-5, PEOE_VSA-6, PEOE_VSA_FNEG, PEOE_VSA_FPNEG, PEOE_VSA_POL, PEOE_VSA_POS, SlogP, SlogP_VSA0, SlogP_VSA1, SlogP_VSA2, SlogP_VSA3, SlogP_VSA8, SMR_VSA3, SMR_VSA6 |
| 6 <sup>#</sup> | DS 2D and MOE 2D | 24                    | ES_Count_ssCH2, QED_HBD, SAScore_Complexity, Num_Rings5, IAC_Mean, a_nN, a_nN, BCUT_SLOGP_1, GCUT_SLOGP_0, GCUT_SLOGP_2, GCUT_SMR_1, opr_brigid, PEOE_VSA+2, PEOE_VSA+3, PEOE_VSA+4, PEOE_VSA0, PEOE_VSA5, PEOE_VSA6, PEOE_VSA_POS, SlogP, SlogP_VSA1, SlogP_VSA2, SlogP_VSA3, SMR_VSA3, SMR_VSA6                   |

<sup>a</sup> 1–3<sup>#</sup>: neuroprotective models against glutamate-induced neurotoxicity (NGN models); 4–6<sup>#</sup>: neuroprotective models against H<sub>2</sub>O<sub>2</sub>-induced neurotoxicity (NHN models).

**2.4.2 Combined naïve Bayesian.** Combined models were developed to integrate the four single classifiers. Consensus scoring or data fusion is used for improving the prediction reliability of single classifier.<sup>37–40</sup> Generally, varying amounts of noise from single classifier can be reduced by combined modelling. In previous study, we developed CC-ANN using four single classifiers fused by artificial neural network to predict the inhibitory effects of a compound toward cdk5 activity.<sup>41</sup> The assay results showed that 9 out of 40 compounds exerted cdk5/p35 inhibitory activities with IC<sub>50</sub> values ranging from 9.23 to 95.57 μM. In this study, the similar approach was adopted. Four single classifiers were combined by fusing with naïve Bayesian algorithm.

The naïve Bayesian classification models were developed using Discovery Studio 4.0. Bayesian is a robust classification approach that can discriminate active compounds from inactive compounds. Generally, the technique is based on the frequency of occurrence of various descriptors which are found in two or more sets of molecules that can discriminate best between these sets. Bayesian classification can process large amounts of data, learn fast, and is tolerant of random noise. For naïve Bayesian classifier, it can generate the posterior probabilities based on the core of function, which are given by eqn (1).

$$P(+|A_1, \dots, A_n) = \frac{P(A_1, \dots, A_n|+)P(+)}{P(A_1, \dots, A_n)} \quad (1)$$

$P(A_1, \dots, A_n|+)$  is the conditional probability of a particular compound being classified as active;  $P(+)$  is the prior probability, a probability induced from a set of compounds in the training set;  $P(A_1, \dots, A_n)$  is the marginal probability of the given descriptors that will occur in the training set.

A more detailed introduction can be found in the following ref. 42–45. In this study, the probability output ( $P_{C+1}$  and  $P_{C-1}$   $i = 1, 2, 3, 4$ ) for each compound was predicted with four single classifiers; then, all of these probability outputs were selected as new descriptors to develop the combined classifiers NB (combined-NB) model that would generate the final combination decision probability ( $P_{C+1}$  and  $P_{C-1}$ ).

## 2.5 Performance evaluation of the models

The quality of the Bayesian classifiers was measured by the quantity of true positives (TP), true negatives (TN), false positives (FP), false negatives (FN), sensitivity (SE), specificity (SP), the overall prediction accuracy (Q) and Matthews correlation coefficient (MCC), which are given by eqn (2)–(6). TP represents the number of active compounds that are predicted as the active. TN represents the number of inactive compounds that are predicted as the inactive. FP stands for the number of inactive compounds that are predicted as the active and FN is the number of active compounds that are predicted as the inactive. SE represents the prediction accuracy for active compounds and SP represents the prediction accuracy for inactive compounds.

$$SE = \frac{TP}{TP + FN} \quad (2)$$

$$SP = \frac{TN}{TN + FP} \quad (3)$$

$$Q^+ = \frac{TP}{TP + FP} \quad (4)$$

$$Q^- = \frac{TN}{TN + FN} \quad (5)$$

$$MCC = \frac{TP \times TN - FN \times FP}{\sqrt{(TP + FN)(TP + FP)(TN + FN)(TN + FP)}} \quad (6)$$

The value of MCC is the most important indicator for the measurement of the quality of binary classification. MCC is essentially a correlation coefficient between the observed and predicted binary classification. Its value ranges from  $-1$  to  $1$ , and a perfect classification gives a correlation coefficient value of  $1$ . In addition, the receiver operating characteristic (ROC) curve was plotted. The ROC curve can graphically present the model behavior of true positive rate against false positive rate in a visual way. Performance was also measured by the area under the ROC curve (AUC). A perfect classifier gives AUC value of  $1$ , whereas random performance gives that of  $0.5$ .

## 2.6 *In vitro* cell-based for neuroprotective assay

**2.6.1 Cell culture and treatment.** PC12 cell line (rat adrenal pheochromocytoma, Institute of Materia Medica, Chinese Academy of Medical Science, Beijing, China) was grown in high glucose DMEM medium supplemented with 5% (v/v) fetal bovine serum (FBS, Gibco, USA), and 10% heat-inactivated horse serum (HS, Gibco, USA). At the treatment, cells were divided into three

groups: (1) control group: no treatment, (2) model group: cells were treated with 40 mM monosodium glutamate<sup>46</sup> (Sigma, USA) or 300  $\mu\text{M}$   $\text{H}_2\text{O}_2$ ,<sup>47</sup> (3) treatment group: cells were pretreated with 30  $\mu\text{M}$  chemicals for 2 h, and then added 40 mM monosodium glutamate or 300  $\mu\text{M}$   $\text{H}_2\text{O}_2$ , respectively. The chemicals showing good anti-oxidative activity (cell damage inhibition rate  $> 40\%$ ), would be diluted for three concentrations (3.3  $\mu\text{M}$ , 10  $\mu\text{M}$  and 30  $\mu\text{M}$ ) at further evaluation.

**2.6.2 MTT assay.** The MTT assay was used to assess anti-oxidant effects. PC12 ( $8 \times 10^3$  per well) were seeded in 96-well plates in 100  $\mu\text{L}$  of culture medium per well for 20 h. When cells were at about 80% confluence, the medium was replaced with DMEM medium. Next, cells were treated with medium containing different concentrations of chemicals for 2 h and then added 300  $\mu\text{M}$   $\text{H}_2\text{O}_2$  or 40  $\text{mmol L}^{-1}$  monosodium glutamate for 22 h respectively. After removal of the medium, 100  $\mu\text{L}$  of MTT ( $0.5 \text{ mg mL}^{-1}$ ) dissolved in medium was added to each well. Following 3 h incubation, medium was replaced with 100  $\mu\text{L}$  of dimethylsulfoxide (DMSO), and absorbance in each well was assessed at 570 nm using an ELISA microplate reader (Spectra Max M5, Molecular Devices, USA). The values of cell survival were normalized against the values for the control group, which was set to 100%. Data were evaluated for statistical significance with *T*-test from GraphPad Prism 6 statistic tool. Differences were considered significant at  $p < 0.05$ .

## 3. Results and discussion

### 3.1 Chemical space analysis

The performance of binary classifiers is related to the chemical diversity of samples utilized in the training set and test set. In general, binary classifiers that only cover a small region of chemical space limit their applications. Tanimoto similarity index and principal component analysis (PCA) are classic methods to

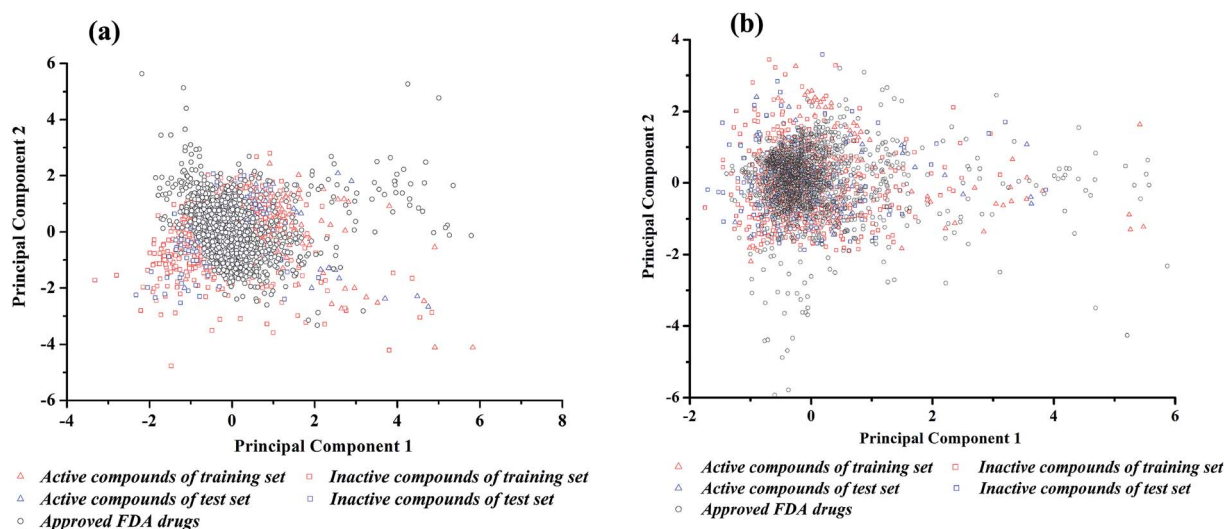


Fig. 2 Diversity distribution of (a) training set ( $n = 1000$  compounds), test set ( $n = 260$  compounds) and approved FDA drugs ( $n = 1670$  compounds) against glutamate-induced neurotoxicity (NGN models), and (b) training set ( $n = 700$  compounds), test set ( $n = 200$  compounds), and approved FDA drugs ( $n = 1670$  compounds) against  $\text{H}_2\text{O}_2$ -induced neurotoxicity (NHN models) as described by the principal component analysis (PCA).

Table 3 Performance of single classification models for the training set and test set using different combinational of molecular properties<sup>a</sup>

| No. | Model   | Descriptors | Training set (5-fold cross validation) |       |                |                |       | Test set |       |                |                |       |
|-----|---------|-------------|----------------------------------------|-------|----------------|----------------|-------|----------|-------|----------------|----------------|-------|
|     |         |             | SE                                     | SP    | Q <sup>+</sup> | Q <sup>-</sup> | MCC   | SE       | SP    | Q <sup>+</sup> | Q <sup>-</sup> | MCC   |
| 1   | NN-a1   | 12          | 0.695                                  | 0.966 | 0.837          | 0.927          | 0.711 | 0.788    | 0.962 | 0.837          | 0.948          | 0.767 |
| 2   | NN-b1   | 23          | 0.755                                  | 0.955 | 0.807          | 0.940          | 0.728 | 0.885    | 0.986 | 0.939          | 0.972          | 0.890 |
| 3   | NN-c1*  | 26          | 0.775                                  | 0.955 | 0.812          | 0.944          | 0.743 | 0.923    | 0.981 | 0.923          | 0.981          | 0.904 |
| 4   | kNN-a1  | 12          | 0.805                                  | 0.911 | 0.694          | 0.949          | 0.679 | 0.981    | 0.947 | 0.823          | 0.995          | 0.871 |
| 5   | kNN-b1  | 23          | 0.850                                  | 0.918 | 0.720          | 0.961          | 0.723 | 1.000    | 0.899 | 0.712          | 1.000          | 0.800 |
| 6   | kNN-c1* | 26          | 0.870                                  | 0.919 | 0.728          | 0.966          | 0.740 | 1.000    | 0.933 | 0.788          | 1.000          | 0.857 |
| 7   | CT-a1   | 12          | 0.660                                  | 0.896 | 0.614          | 0.913          | 0.542 | 0.827    | 0.933 | 0.754          | 0.956          | 0.734 |
| 8   | CT-b1   | 23          | 0.700                                  | 0.903 | 0.642          | 0.923          | 0.584 | 0.923    | 0.928 | 0.762          | 0.980          | 0.794 |
| 9   | CT-c1*  | 26          | 0.735                                  | 0.898 | 0.642          | 0.931          | 0.602 | 0.904    | 0.933 | 0.770          | 0.975          | 0.790 |
| 10  | RF-a1   | 12          | 0.415                                  | 0.971 | 0.783          | 0.869          | 0.502 | 0.538    | 0.986 | 0.903          | 0.895          | 0.647 |
| 11  | RF-b1   | 23          | 0.615                                  | 0.973 | 0.848          | 0.910          | 0.667 | 0.904    | 0.976 | 0.904          | 0.976          | 0.880 |
| 12  | RF-c1*  | 26          | 0.690                                  | 0.949 | 0.771          | 0.924          | 0.666 | 0.904    | 0.976 | 0.904          | 0.976          | 0.880 |
| 13  | NN-a2   | 12          | 0.521                                  | 0.959 | 0.760          | 0.889          | 0.559 | 0.725    | 0.969 | 0.853          | 0.934          | 0.739 |
| 14  | NN-b2*  | 26          | 0.771                                  | 0.975 | 0.885          | 0.945          | 0.787 | 0.875    | 0.975 | 0.897          | 0.969          | 0.858 |
| 15  | NN-c2   | 24          | 0.714                                  | 0.966 | 0.840          | 0.931          | 0.724 | 0.925    | 0.988 | 0.949          | 0.981          | 0.921 |
| 16  | kNN-a2  | 12          | 0.714                                  | 0.914 | 0.676          | 0.928          | 0.616 | 0.950    | 0.944 | 0.809          | 0.987          | 0.843 |
| 17  | kNN-b2* | 26          | 0.857                                  | 0.932 | 0.759          | 0.963          | 0.755 | 1.000    | 0.938 | 0.800          | 1.000          | 0.866 |
| 18  | kNN-c2  | 24          | 0.829                                  | 0.923 | 0.730          | 0.956          | 0.718 | 1.000    | 0.975 | 0.909          | 1.000          | 0.941 |
| 19  | CT-a2   | 12          | 0.607                                  | 0.888 | 0.574          | 0.900          | 0.485 | 0.900    | 0.888 | 0.667          | 0.973          | 0.710 |
| 20  | CT-b2*  | 26          | 0.721                                  | 0.932 | 0.727          | 0.930          | 0.655 | 0.900    | 0.913 | 0.720          | 0.973          | 0.751 |
| 21  | CT-c2   | 24          | 0.779                                  | 0.902 | 0.665          | 0.942          | 0.643 | 0.950    | 0.888 | 0.679          | 0.986          | 0.746 |
| 22  | RF-a2   | 12          | 0.371                                  | 0.964 | 0.722          | 0.860          | 0.442 | 0.525    | 0.981 | 0.875          | 0.892          | 0.623 |
| 23  | RF-b2*  | 26          | 0.771                                  | 0.946 | 0.783          | 0.943          | 0.722 | 0.900    | 0.950 | 0.818          | 0.974          | 0.821 |
| 24  | RF-c2   | 24          | 0.707                                  | 0.954 | 0.792          | 0.929          | 0.690 | 0.850    | 0.956 | 0.829          | 0.962          | 0.799 |

<sup>a</sup> 1–12: neuroprotective models against glutamate-induced neurotoxicity (NGN models); 13–24: neuroprotective models against H<sub>2</sub>O<sub>2</sub>-induced neurotoxicity (NHN models); a: models built by DS\_2D descriptors; b: models built by MOE\_2D descriptors; c: models built by DS\_MOE 2D descriptors.

explore the diversity of compounds within a chemical data set. The Tanimoto similarity analysis was performed with the fingerprint of ECFP<sub>2</sub>. As shown in Table 1, for neuroprotective models against glutamate-induced neurotoxicity (NGN models), the Tanimoto index is 0.125 for training set and 0.132 for test set. For neuroprotective models against H<sub>2</sub>O<sub>2</sub>-induced neurotoxicity (NHN models), the Tanimoto index is 0.142 for training set and 0.162 for test set. Consequently, the entire data set was diverse enough.

Principal component analysis (PCA) was another approach to investigate the chemical spaces of the training set and test set.<sup>48</sup> For NGN and NHN models, the input variables were the 26 DS\_MOE and 26 MOE 2D descriptors selected by Pearson correlation analysis and genetic search, respectively. Subsequently, 1630 FDA-approved drugs were downloaded from DrugBank,<sup>49</sup> and the same properties were calculated. According to the chemical space defined by PCA (Fig. 2), there are enough diverse chemical space distributions for all compounds, and most of the compounds in test set are well within the chemical space of the training set. At the same time, there are obvious overlaps between the compounds in dataset and FDA-approved drugs in chemical space, which implies that most of the compounds have drug potential.

### 3.2 Performance of binary classification models by single classifier

A total of 24 single classifiers in this study (12 for each data set) were initially generated using NN, kNN, CT and RF algorithms

with three sets of descriptors. Subsequently, the internal 5-fold cross validation was adopted to evaluate the performance. Additionally, the models were used to predict corresponding test set comprising 260 and 200 compounds. The performance of all the single classifiers is given in Table 3.

Among the 12 NGN models, the MCC values of 5-fold cross validation ranged from 0.502 to 0.743, whereas those of test set ranged from 0.647 to 0.904. The best single classifier was NN-c1, which was developed by neural network using 26 DS\_MOE descriptors. Regarding to the 12 NHN models, the MCC values of 5-fold cross validation varied from 0.442 to 0.787, whereas those of test set varied from 0.623 to 0.941. The best performance was achieved by NN-b2, neural network using 26 MOE descriptors. These data indicated that the overall predictive accuracies of 24 single classifiers from NGN and NHN were not high but acceptable. The detailed performance of the 24 single classifiers are given in Table S5.†

To compare the performance of single models from different algorithms, the average MCC values divided by three sets of descriptors are given in Fig. 3. For NGN single models (Fig. 3a), the performances of models from neural network (NN) and *k* near neighbour (*k*NN) are superior to those from classification tree (CT) and random forest (RF). The best performance is achieved by NN algorithm, with the average MCC value of 0.727 and 0.854 from 5-fold cross validation and test set, respectively. For NHN single classifiers (Fig. 3b), NN and *k*NN perform better than CT and RF, which is similar to NGN models. Among four different

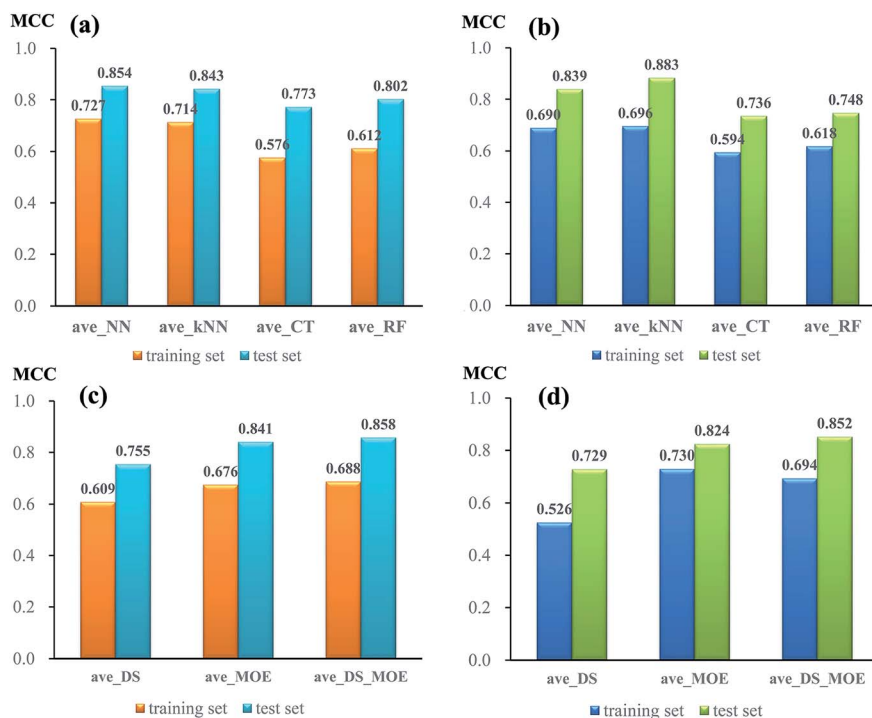


Fig. 3 The comparison of average MCC values made by different algorithms (a and b) and different sets of descriptors (c and d) against glutamate-induced neurotoxicity (a and c) and H<sub>2</sub>O<sub>2</sub>-induced neurotoxicity (b and d) on training set and test set.

algorithms, *k*NN obtains the highest average MCC value of 0.696 from 5-fold cross validation and 0.883 from test set.

In addition, the performances of models from different sets of descriptors are also compared. As given in Fig. 3c, for single NGN models, the average MCC values from three sets of descriptors (DS, MOE, and DS\_MOE) are 0.609, 0.679, and 0.688 for 5-fold cross validation as well as 0.755, 0.841, and 0.858 for test set. Obviously, here the four models derived from DS\_MOE descriptors perform best and are chosen for further integration. However, for single NHN models, it is difficult to judge which performs better between models using MOE or DS\_MOE descriptors. As presented in Fig. 3d, the models using DS\_MOE descriptors have a higher average MCC value of 0.852 for test set, whereas the models using MOE descriptors get a better average MCC value of 0.730 in 5-fold cross validation for the training set. Considering that the models from MOE descriptors have both the desired MCC values (0.730 and 0.824) for 5-fold cross validation and test set, the single classifiers using MOE descriptors are selected for further analysis.

### 3.3 Performance of combined naïve Bayesian models

As discussed above, based on the two best sets of descriptors (DS\_MOE descriptors and MOE descriptors), 4 single classifiers (NN-c1, *k*NN-c1, CT-c1, and RF-c1) from NGN models were chosen to develop the combined naïve Bayesian model combined-NB-1, while another 4 single classifiers (NN-b2, *k*NN-b2, CT-b2 and RF-b2) from NHN models were selected to build combined-NB-2. To compare the performance between single classifiers and combined naïve Bayesian model, the MCC values

and AUC values *via* receiver operating characteristic (ROC) plot were calculated.

As given in Fig. 4a and b, the performance of combined-NB-1 (MCC = 0.814) is better than any single classifiers (MCC ranging from 0.602 to 0.743) on 5-fold cross validation. At the same time, the MCC value of combined NB-1 (0.923) on test set is also significantly higher than that of 4 single classifiers (MCC ranging from 0.790 to 0.904). A similar phenomenon occurs in combined-NB-2 (Fig. 4c and d). Combined-NB-2 model obtains MCC values of 0.836 and 0.878 on 5-fold cross validation and test set, respectively, which is much higher than those of single classifiers based on 26 MOE descriptors.

AUC values *via* receiver operating characteristic (ROC) plot were also compared in Fig. 5. As shown in Fig. 5a and b, the combined-NB-1 model achieves the highest AUC value of 0.958 and 0.999 among the five models on 5-fold cross validation and test set, respectively. Similarly, the combined-NB-2 obtains the highest AUC values of 0.975 and 0.999 among the five models. To sum up, after integrating different single classifiers, the combined NB models can improve the predictive performance obviously.

In order to further improve the performance of combined-NB-1 and combined-NB-2, different molecular fingerprints, together with 8 probabilities outputted by 4 single classifiers, were used simultaneously as the descriptors in Bayesian analysis to build new prediction models. The statistical results for these Bayesian classifiers are listed in Tables 4 and S6.† For NGN models, the combined-NB models using fingerprints (no. 2–13), have MCC values ranging from 0.818 to 0.975 on 5-fold

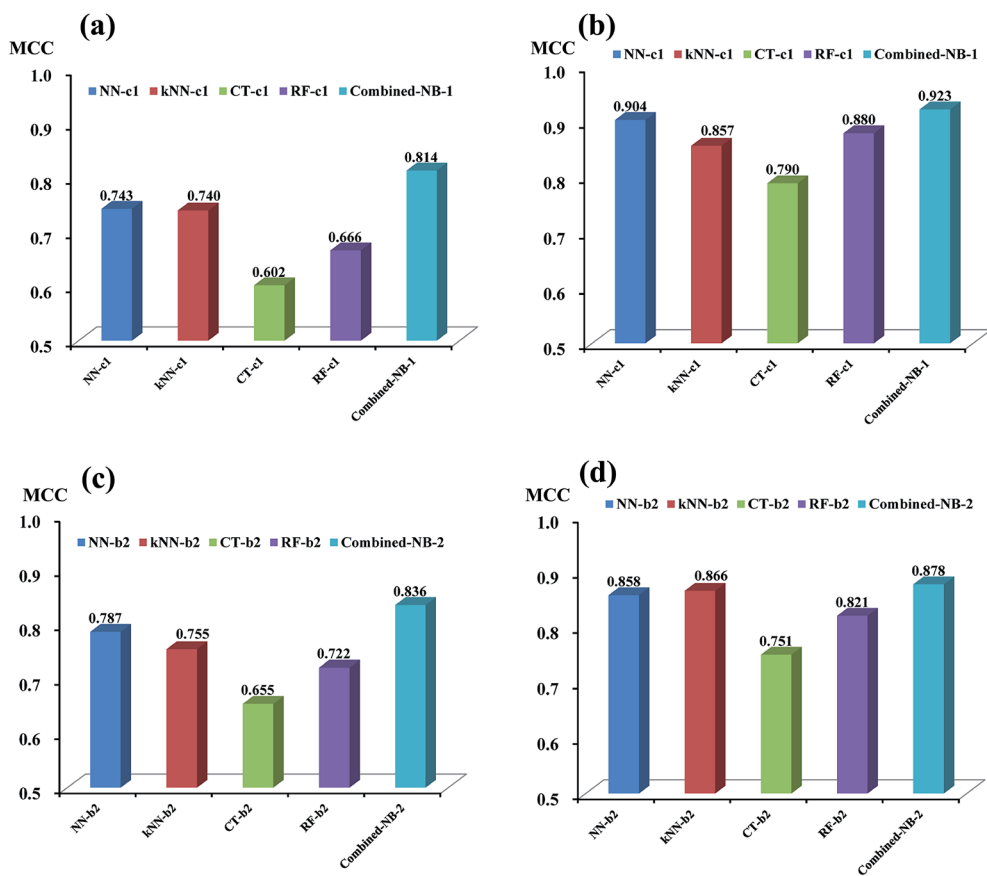


Fig. 4 The comparison of MCC value made by four single classifiers and combined-NB model against glutamate-induced neurotoxicity (a and b) and H<sub>2</sub>O<sub>2</sub>-induced neurotoxicity (c and d) on training set (a and c) and test set (b and d).

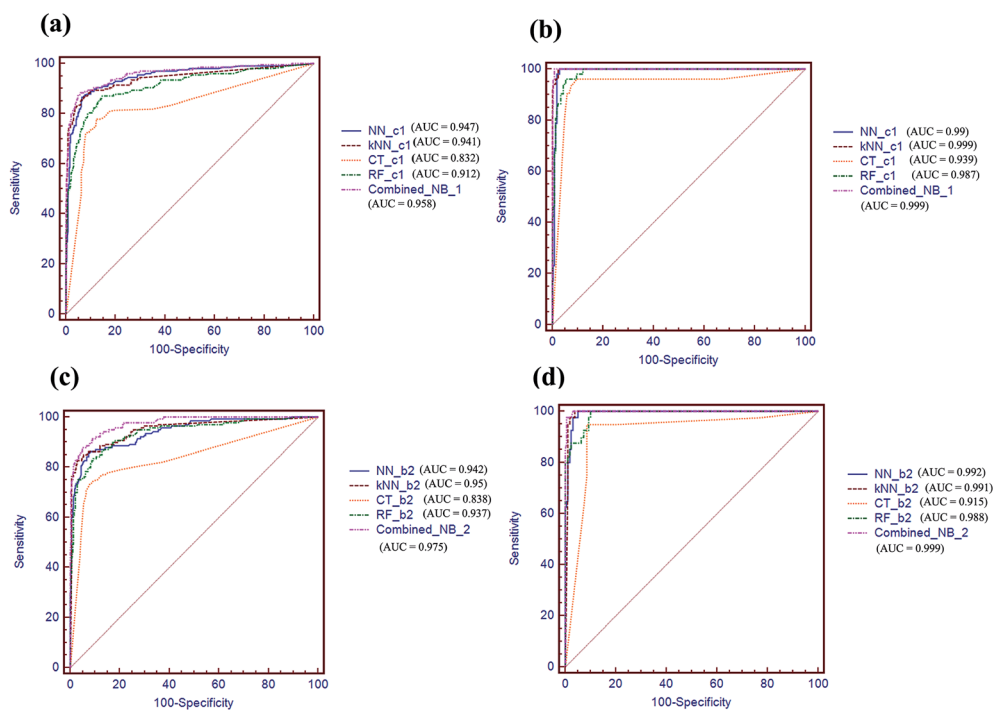


Fig. 5 The comparison of AUC value via receiver operating characteristic (ROC) plot made by four single classifiers and combined-NB model against glutamate-induced neurotoxicity (a and b) and H<sub>2</sub>O<sub>2</sub>-induced neurotoxicity (c and d) on training set (a and c) and test set (b and d).



**Table 4** Performance of the 26 Bayesian classification models for the training set and test set using different combinational of output probabilities and fingerprints<sup>a</sup>

| No. | Model    | Training set (5-fold cross validation) |       |                |                |       | Test set |       |                |                |       |
|-----|----------|----------------------------------------|-------|----------------|----------------|-------|----------|-------|----------------|----------------|-------|
|     |          | SE                                     | SP    | Q <sup>+</sup> | Q <sup>-</sup> | MCC   | SE       | SP    | Q <sup>+</sup> | Q <sup>-</sup> | MCC   |
| 1   | NB       | 0.875                                  | 0.955 | 0.829          | 0.968          | 0.814 | 1.000    | 0.966 | 0.881          | 1.000          | 0.923 |
| 2   | NB+ECFP4 | 0.940                                  | 0.986 | 0.945          | 0.985          | 0.928 | 1.000    | 0.962 | 0.867          | 1.000          | 0.913 |
| 3   | NB+ECFP6 | 0.950                                  | 0.998 | 0.990          | 0.988          | 0.962 | 1.000    | 0.986 | 0.945          | 1.000          | 0.965 |
| 4   | NB+EPFP4 | 0.925                                  | 0.940 | 0.794          | 0.980          | 0.818 | 1.000    | 0.938 | 0.800          | 1.000          | 0.866 |
| 5   | NB+EPFP6 | 0.965                                  | 0.933 | 0.781          | 0.991          | 0.832 | 0.981    | 0.938 | 0.797          | 0.995          | 0.853 |
| 6   | NB+FCFP4 | 0.895                                  | 0.989 | 0.952          | 0.974          | 0.905 | 1.000    | 0.990 | 0.963          | 1.000          | 0.977 |
| 7   | NB+FCFP6 | 0.970                                  | 0.974 | 0.902          | 0.992          | 0.919 | 1.000    | 0.995 | 0.981          | 1.000          | 0.988 |
| 8   | NB+FPFP4 | 0.940                                  | 0.950 | 0.825          | 0.984          | 0.849 | 0.981    | 0.981 | 0.927          | 0.995          | 0.942 |
| 9   | NB+FPFP6 | 0.970                                  | 0.963 | 0.866          | 0.992          | 0.895 | 0.962    | 0.971 | 0.893          | 0.990          | 0.908 |
| 10  | NB+LCFP4 | 0.960                                  | 0.978 | 0.914          | 0.990          | 0.921 | 1.000    | 1.000 | 1.000          | 1.000          | 1.000 |
| 11  | NB+LCFP6 | 0.965                                  | 0.981 | 0.928          | 0.991          | 0.933 | 1.000    | 1.000 | 1.000          | 1.000          | 1.000 |
| 12  | NB+LPFP4 | 0.985                                  | 0.993 | 0.970          | 0.996          | 0.972 | 0.981    | 0.986 | 0.944          | 0.995          | 0.953 |
| 13  | NB+LPFP6 | 0.980                                  | 0.995 | 0.980          | 0.995          | 0.975 | 1.000    | 0.976 | 0.912          | 1.000          | 0.944 |
| 14  | NB       | 0.843                                  | 0.975 | 0.894          | 0.961          | 0.836 | 1.000    | 0.931 | 0.784          | 1.000          | 0.855 |
| 15  | NB+ECFP4 | 0.936                                  | 0.996 | 0.985          | 0.984          | 0.950 | 1.000    | 0.956 | 0.851          | 1.000          | 0.902 |
| 16  | NB+ECFP6 | 0.929                                  | 1.000 | 1.000          | 0.982          | 0.955 | 1.000    | 0.944 | 0.816          | 1.000          | 0.878 |
| 17  | NB+EPFP4 | 0.929                                  | 0.927 | 0.760          | 0.981          | 0.796 | 0.925    | 0.906 | 0.712          | 0.980          | 0.758 |
| 18  | NB+EPFP6 | 0.964                                  | 0.930 | 0.776          | 0.990          | 0.828 | 0.975    | 0.906 | 0.722          | 0.993          | 0.794 |
| 19  | NB+FCFP4 | 0.993                                  | 0.925 | 0.768          | 0.998          | 0.839 | 1.000    | 0.956 | 0.851          | 1.000          | 0.902 |
| 20  | NB+FCFP6 | 0.943                                  | 0.991 | 0.964          | 0.986          | 0.942 | 1.000    | 0.969 | 0.889          | 1.000          | 0.928 |
| 21  | NB+FPFP4 | 0.971                                  | 0.884 | 0.677          | 0.992          | 0.756 | 0.975    | 0.881 | 0.672          | 0.993          | 0.755 |
| 22  | NB+FPFP6 | 0.914                                  | 0.970 | 0.883          | 0.978          | 0.872 | 0.975    | 0.925 | 0.765          | 0.993          | 0.826 |
| 23  | NB+LCFP4 | 0.986                                  | 0.980 | 0.926          | 0.996          | 0.944 | 1.000    | 0.950 | 0.833          | 1.000          | 0.890 |
| 24  | NB+LCFP6 | 0.986                                  | 0.986 | 0.945          | 0.996          | 0.956 | 1.000    | 0.956 | 0.851          | 1.000          | 0.902 |
| 25  | NB+LPFP4 | 0.986                                  | 0.964 | 0.873          | 0.996          | 0.909 | 1.000    | 0.938 | 0.800          | 1.000          | 0.866 |
| 26  | NB+LPFP6 | 0.971                                  | 0.986 | 0.944          | 0.993          | 0.947 | 1.000    | 0.944 | 0.816          | 1.000          | 0.878 |

<sup>a</sup> 1–13: combined naïve Bayesian models for neuroprotection against glutamate-induced neurotoxicity; 14–26: combined NB models for neuroprotection against H<sub>2</sub>O<sub>2</sub>-induced neurotoxicity.

cross validation, which are much higher than that of combined-NB-1 (no. 1). Given the balance performance between training set and test set, NB-1-LPFP4 (no. 12) which obtains corresponding MCC values of 0.972 and 0.953 on 5-fold cross validation and test set, is considered as the best model to predict neuroprotective activity against glutamate-induced neurotoxicity. For NHH models (no. 14–26), except for NB-2-EPFP4 (no. 17) and NB-2-FPFP4 (no. 21), all of the other ten models using fingerprints perform better than combined-NB-2 (no. 14) on 5-fold cross validation. Similarly, NB-2-LCFP6 (no. 24) with corresponding MCC values of 0.956 and 0.902 on 5-fold cross validation and test set, is recognized as the best model to predict neuroprotective activity against H<sub>2</sub>O<sub>2</sub>-induced neurotoxicity. Consequently, the addition of fingerprint can improve the performance of combined NB-1 and NB-2 models.

The Bayesian scores based on NB-1-LPFP4 and NB-2-LCFP6 were used to evaluate the discrimination of active compounds from inactive compounds *via* bimodal histograms of the training and test data sets (Fig. 6). As given in Fig. 6a and b, for NB-1-LPFP4 model, the *p* value associated with the difference in the mean Bayesian score of training set active *versus* inactive compounds is 0 at the 95% confidence level as well as *p* value of  $5.12 \times 10^{-83}$  on test set, suggesting that the two distributions were significantly different. In a similar way, for NB-2-LCFP6

model (Fig. 6c and d), the corresponding *p* values are  $3.39 \times 10^{-261}$  and  $2.17 \times 10^{-79}$  on training set and test set, implying that Bayesian score can discriminate active compounds from inactive compounds greatly. Inspired by the two best models, we found the Bayesian score of neuroprotective agents tended to have more positive value, while the Bayesian score of inactive compounds inclined to have more negative value. The Bayesian score of a compound could be a quantitation standard to choose potential compounds as neuroprotective agents in virtual screening.

### 3.4 Y-scrambling

As discussed above, NB-1-LPFP4 and NB-2-LCFP6 were regarded as the best neuroprotective models against glutamate or H<sub>2</sub>O<sub>2</sub>-induced neurotoxicity, respectively. Y-scrambling was performed to prove that it was not a result of chance correlation to have good performance for the best models. The steps are as follows. First, the activity (1 or 0) column was randomly shuffled in the training set molecules, and a new Bayesian model was developed. The procedure was repeated 50 times and the new models were expected to have low Matthews correlation coefficient (MCC) and prediction accuracy (*Q*). The resulting MCC and *Q* for the test set are presented in Fig. S1,<sup>†</sup> from which all the scrambled models have a MCC less than 0.3 and *Q* less than

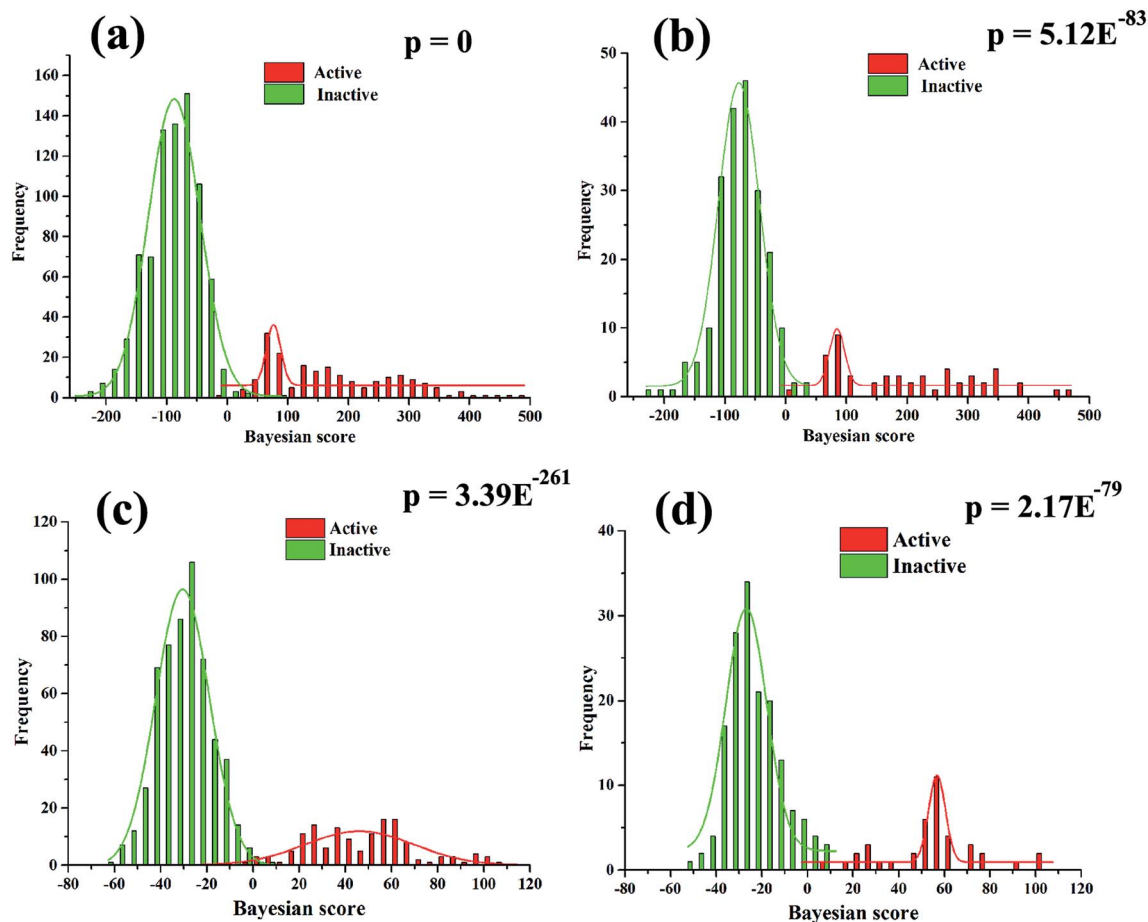


Fig. 6 The distributions of Bayesian score predicted by the Bayesian classifier NB-1-LPFP4 (a and b) and NB-2-LCFP6 (c and d) on training set (a and c) and test set (b and d).

0.8, whereas the values of MCC and Q of NB-1-LPFP4 and NB-2-LCFP6 are significantly greater.

### 3.5 Applicability domain of the generated QSAR

An extremely important issue for classification model is the definition of the applicability domain (AD). The reason is that the reliable QSAR predictions are limited generally to the chemicals that are structurally similar to the training compounds. If the test compounds are too far away from the chemical space of AD, the predictions are usually unreliable. There are several measures for the definition of applicability

domain.<sup>50–53</sup> In this study, stepwise approach was used to determine the two best models' AD with two domain layers (Fig. S2†). The first domain layer (named “parameter range”) was extracted based on molecular weight (MW) and  $\log(K_{ow})$  with correct predicted chemicals from training set (called good fragments). The second domain layer was “structure domain” which was extracted by the atom-centered fragment method. The atom-centered fragment is a topological sphere with center a selected atom and radius specified in any atom distance. In this work, the parameter range for NB-1-LPFP4 is  $MW[124.17, 862.90]$  as well as  $\log(K_{ow})[-8.63, 12.96]$ , while that for NB-2-

Table 5 Numbers of chemicals were determined to be in domain (ID) and out of domain (OD) in the training set and test sets using application domain assessment methods<sup>a</sup>

| Model      | Training set   |             |       |                    |             |       | Test set       |             |       |                    |             |       |
|------------|----------------|-------------|-------|--------------------|-------------|-------|----------------|-------------|-------|--------------------|-------------|-------|
|            | In domain (ID) |             |       | Out of domain (OD) |             |       | In domain (ID) |             |       | Out of domain (OD) |             |       |
|            | $N_p$          | $N_{non-p}$ | Total | $N_p$              | $N_{non-p}$ | Total | $N_p$          | $N_{non-p}$ | Total | $N_p$              | $N_{non-p}$ | Total |
| NB-1-LPFP4 | 199            | 797         | 996   | 1                  | 3           | 4     | 52             | 178         | 230   | 0                  | 30          | 30    |
| NB-2-LCFP6 | 140            | 557         | 697   | 0                  | 3           | 3     | 40             | 148         | 188   | 0                  | 12          | 12    |

<sup>a</sup>  $N_p$ : the number of positive compounds;  $N_{non-p}$ : the number of decoy compounds; NB-1-LPFP4: the best model for neuroprotection against glutamate-induced neurotoxicity; NB-2-LCFP6: the best model for neuroprotection against  $H_2O_2$ -induced neurotoxicity.

LCFP6 is MW[157.17, 1165.01] as well as  $\log(K_{ow})[-12.80, 11.31]$ . AD analysis results for training set and test set is presented in Table 5. It can be easily seen that all active compounds of test set are located in domain although a small number of the decoy compounds are located out of domain. Consequently, the predictions of the two best models (NB-1-LPFP4 and NB-2-LCFP6) are reliable.

### 3.6 Analysis of the important fragments given by naïve Bayesian classifier

To further explore favorable structural fragments for neuroprotective compounds, the good fragments as well as the frequency of each fragment given by NB-1-LPFP4 and NB-2-LCFP6 classifiers were summarized in Fig. 7, which were ranked by their Bayesian score. It may be useful for neuroprotective compounds design. In Fig. 7a, as to the model against glutamate-induced neurotoxicity (NB-1-LPFP4), all of the privilege fragments only

contain three elements (C, H, and O), and most of fragments with oxygen atom belong to the family of esters. Therefore, hydrophobic interactions may be the main driving force for these fragments to favorably bind to the targets related to neuroprotection. As shown in Fig. 7b, for the neuroprotective compounds against  $H_2O_2$ -induced neurotoxicity (NB-2-LCFP6), the favorable fragments are mainly composed of sulfonic amides, polyphenols and the fragments with unsaturated side chains. This is reasonable because these groups are functional groups with reducibility which are more likely antioxidants. It is well known most of antioxidants such as vitamin E have neuroprotection against  $H_2O_2$ -induced neurotoxicity. Besides, for sulfonic amides and polyphenols, hydrogen bonding may play a significant role in binding to the neuroprotective targets. For example, there are 14 sulfonic amides out of 140 known neuroprotective compounds on training set, while there are 8 out of 40 known neuroprotective compounds on test set.

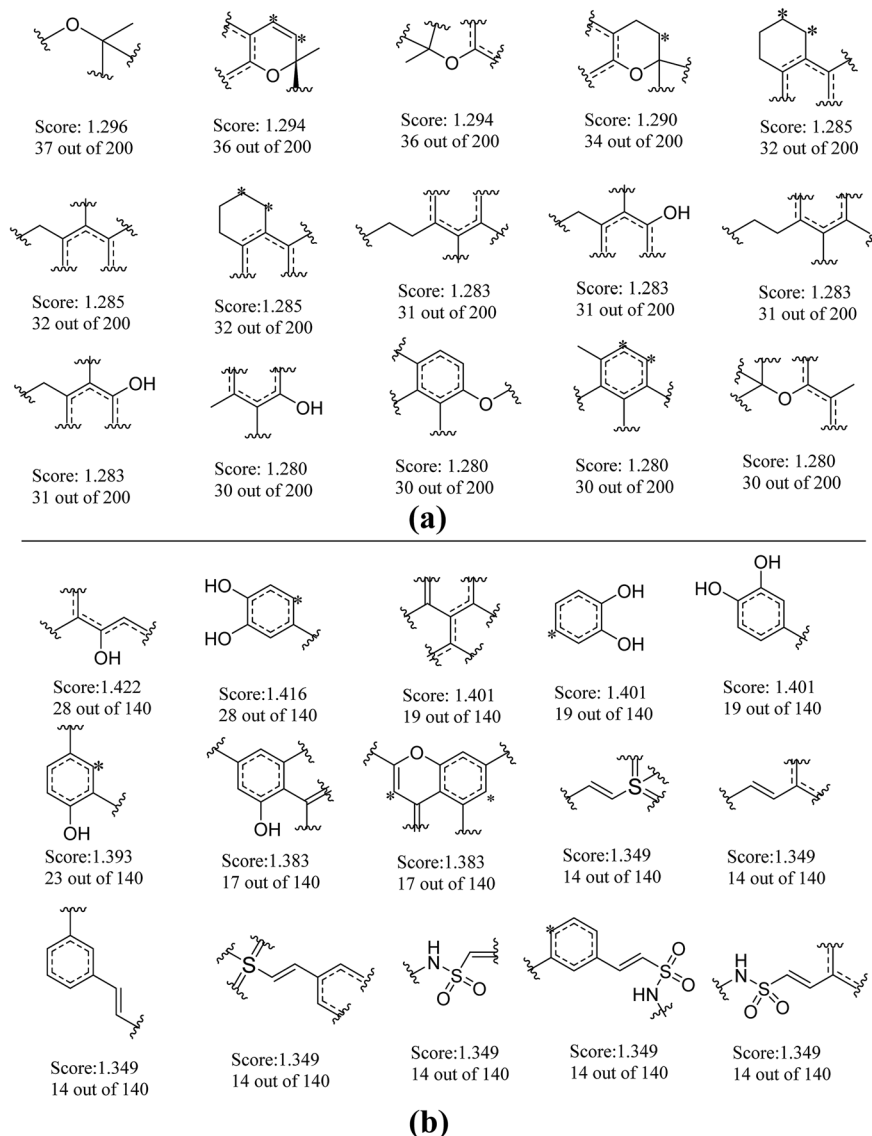


Fig. 7 Examples of the top 30 good fragments estimated by NB-1-LPFP4 (a) and NB-2-LCFP6 (b) models. The Bayesian score (Score) and the frequency of each fragment in active compounds are given.

Table 6 Neuroprotective effects of compounds on monosodium glutamate or H<sub>2</sub>O<sub>2</sub>-induced neurotoxicity on PC12 cells

| Compound <sup>a</sup> | Monosodium glutamate (40 mM) test concentration (μM) |                           |                            | H <sub>2</sub> O <sub>2</sub> (300 μM) test concentration (μM) |                            |                             |
|-----------------------|------------------------------------------------------|---------------------------|----------------------------|----------------------------------------------------------------|----------------------------|-----------------------------|
|                       | 3.3 μM                                               | 10 μM                     | 30 μM                      | 3.3 μM                                                         | 10 μM                      | 30 μM                       |
| J10216                | 76.41 ± 1.84                                         | 84.57 ± 4.58 <sup>d</sup> | 81.75 ± 3.43 <sup>d</sup>  | 82.54 ± 1.53                                                   | 83.31 ± 4.87               | 92.83 ± 0.025 <sup>c</sup>  |
| J10233                | 76.28 ± 3.18                                         | 83.81 ± 0.19 <sup>e</sup> | 108.43 ± 1.76 <sup>e</sup> | 68.73 ± 2.14                                                   | 80.14 ± 1.45               | 133.15 ± 3.65 <sup>c</sup>  |
| J11762                | 63.29 ± 2.12                                         | 68.41 ± 2.67              | 89.24 ± 0.40 <sup>e</sup>  | 91.82 ± 0.99 <sup>c</sup>                                      | 100.03 ± 2.58 <sup>c</sup> | 123.11 ± 0.83 <sup>c</sup>  |
| J12146                | 70.05 ± 4.61                                         | 75.97 ± 0.34              | 79.18 ± 1.73 <sup>d</sup>  | 82.14 ± 1.00                                                   | 86.47 ± 2.27 <sup>b</sup>  | 82.19 ± 2.78                |
| J14156                | 67.83 ± 1.03                                         | 73.66 ± 1.01              | 79.28 ± 3.08 <sup>d</sup>  | 83.04 ± 3.35                                                   | 91.16 ± 1.62 <sup>c</sup>  | 100.63 ± 0.48 <sup>c</sup>  |
| J14572                | 77.58 ± 1.40 <sup>d</sup>                            | 78.66 ± 1.76 <sup>d</sup> | 90.23 ± 1.25 <sup>e</sup>  | 87.12 ± 1.17 <sup>b</sup>                                      | 93.04 ± 1.35 <sup>c</sup>  | 106.28 ± 1.20 <sup>c</sup>  |
| J14581                | 71.78 ± 0.55                                         | 73.38 ± 0.59              | 77.41 ± 0.08 <sup>d</sup>  | 80.11 ± 0.66                                                   | 85.49 ± 5.54               | 88.12 ± 3.58 <sup>b</sup>   |
| J14590                | 71.01 ± 3.94                                         | 83.56 ± 2.68 <sup>e</sup> | 92.89 ± 2.35 <sup>e</sup>  | —                                                              | —                          | —                           |
| J14591                | 71.92 ± 1.24                                         | 77.51 ± 0.48 <sup>d</sup> | 81.85 ± 2.95 <sup>d</sup>  | 99.66 ± 3.28 <sup>c</sup>                                      | 100.90 ± 1.5 <sup>c</sup>  | 103.70 ± 4.83 <sup>c</sup>  |
| J14593                | 71.43 ± 5.6                                          | 78.36 ± 0.81 <sup>d</sup> | 86.35 ± 2.88 <sup>e</sup>  | 78.01 ± 0.28                                                   | 92.86 ± 2.3 <sup>c</sup>   | 84.86 ± 1.12                |
| J14691                | 76.25 ± 2.03                                         | 90.72 ± 1.50 <sup>e</sup> | 101.70 ± 5.7 <sup>e</sup>  | 77.76 ± 0.43                                                   | 77.28 ± 2.58               | 92.37 ± 4.19 <sup>c</sup>   |
| J18811                | 80.72 ± 2.96 <sup>d</sup>                            | 93.91 ± 0.78 <sup>e</sup> | 128.07 ± 5.66 <sup>e</sup> | 86.63 ± 1.49 <sup>b</sup>                                      | 93.69 ± 2.5 <sup>c</sup>   | 93.06 ± 2.49 <sup>c</sup>   |
| J18836                | 85.51 ± 3.20 <sup>d</sup>                            | 92.82 ± 3.05 <sup>e</sup> | 83.62 ± 0.91 <sup>e</sup>  | 76.27 ± 0.68                                                   | 92.10 ± 1.52 <sup>c</sup>  | 62.22 ± 0.51                |
| J18842                | 71.41 ± 0.53                                         | 76.12 ± 2.06              | 81.26 ± 0.65 <sup>d</sup>  | 79.74 ± 5.83                                                   | 98.89 ± 3.04 <sup>c</sup>  | 104.32 ± 2.30 <sup>c</sup>  |
| J18879                | 84.44 ± 3.43 <sup>d</sup>                            | 86.11 ± 2.05 <sup>e</sup> | 99.67 ± 0.91 <sup>e</sup>  | 59.34 ± 5.38                                                   | 66.92 ± 4.42               | 78.79 ± 4.86                |
| J27114                | 69.04 ± 0.067                                        | 74.70 ± 1.04              | 84.33 ± 0.91 <sup>e</sup>  | 80.78 ± 0.015                                                  | 83.85 ± 1.38               | 98.38 ± 0.06 <sup>c</sup>   |
| J27115                | 76.16 ± 0.28                                         | 80.16 ± 4.31              | 86.13 ± 3.59 <sup>d</sup>  | 81.97 ± 1.16                                                   | 75.01 ± 5.90               | 91.12 ± 2.52 <sup>c</sup>   |
| J27118                | 82.64 ± 0.65 <sup>d</sup>                            | 81.09 ± 1.78 <sup>d</sup> | 84.19 ± 1.94 <sup>d</sup>  | 90.06 ± 2.97 <sup>b</sup>                                      | 91.65 ± 0.87 <sup>c</sup>  | 92.13 ± 0.62 <sup>c</sup>   |
| J27151                | 73.43 ± 4.87                                         | 77.41 ± 2.62              | 103.11 ± 6.28 <sup>e</sup> | 81.64 ± 0.28                                                   | 88.62 ± 6.16               | 114.63 ± 4.03 <sup>c</sup>  |
| J27152                | 77.25 ± 3.28                                         | 86.55 ± 1.93 <sup>e</sup> | 94.63 ± 2.31 <sup>e</sup>  | 78.08 ± 1.31                                                   | 86.15 ± 3.80 <sup>b</sup>  | 94.02 ± 3.53 <sup>b</sup>   |
| J27153                | 69.65 ± 3.11                                         | 79.43 ± 1.70 <sup>d</sup> | 98.63 ± 0.49 <sup>e</sup>  | 94.83 ± 2.95 <sup>c</sup>                                      | 113.56 ± 4.94 <sup>c</sup> | 110.81 ± 4.68 <sup>c</sup>  |
| J27155                | 72.49 ± 3.63                                         | 81.65 ± 2.91 <sup>d</sup> | 90.11 ± 3.82 <sup>e</sup>  | 58.63 ± 4.67                                                   | 86.97 ± 3.23               | 110.04 ± 10.33 <sup>b</sup> |
| J27167                | 67.07 ± 6.79                                         | 59.79 ± 0.41              | 85.76 ± 3.28 <sup>d</sup>  | 88.41 ± 2.99 <sup>b</sup>                                      | 98.29 ± 2.3 <sup>c</sup>   | 88.32 ± 1.18 <sup>b</sup>   |
| J27198                | 67.79 ± 3.79                                         | 65.39 ± 1.01              | 85.54 ± 1.11 <sup>e</sup>  | 61.55 ± 6.34                                                   | 82.29 ± 0.43               | 91.26 ± 2.60 <sup>b</sup>   |
| J27706                | 80.71 ± 1.52 <sup>d</sup>                            | 74.77 ± 0.04              | 92.34 ± 4.37 <sup>e</sup>  | 81.32 ± 5.78                                                   | 82.40 ± 4.15               | 84.12 ± 0.27                |
| J27709                | 67.02 ± 1.46                                         | 80.33 ± 0.35 <sup>d</sup> | 80.12 ± 2.72               | 87.44 ± 0.95 <sup>b</sup>                                      | 87.27 ± 6.11               | 96.80 ± 1.70 <sup>c</sup>   |
| J32899                | 61.74 ± 2.22                                         | 68.86 ± 3.08              | 80.82 ± 1.96 <sup>d</sup>  | 83.78 ± 3.21                                                   | 91.67 ± 1.98 <sup>c</sup>  | 86.28 ± 5.94                |
| J100313               | 66.93 ± 1.91                                         | 75.12 ± 3.58              | 80.31 ± 4.01               | 77.44 ± 0.43                                                   | 86.07 ± 1.00               | 90.83 ± 0.95 <sup>c</sup>   |
| Vitamin E             | 79.66 ± 3.77                                         | 85.22 ± 3.87 <sup>d</sup> | 92.68 ± 5.10 <sup>e</sup>  | 91.29 ± 4.32 <sup>b</sup>                                      | 97.67 ± 4.44 <sup>b</sup>  | 106.22 ± 5.85 <sup>c</sup>  |

<sup>a</sup> The data (cell viability, measured by MTT assay) were normalized and expressed as a percentage of the control group, which was set to 100%. Degree of damage of H<sub>2</sub>O<sub>2</sub> was 69.24 ± 3.09, and degree of damage of monosodium glutamate was 66.05 ± 1.82. Data expressed as means ± SEM. Three independent experiments were carried out. <sup>b</sup> *P* < 0.05. <sup>c</sup> *P* < 0.01 vs. H<sub>2</sub>O<sub>2</sub> group. <sup>d</sup> *P* < 0.05. <sup>e</sup> *P* < 0.01 vs. monosodium glutamate group.

### 3.7 Virtual screening of an in-house database for neuroprotective agents

Based on the two best neuroprotective models (NB-1-LPFP4 and NB-2-LCFP6), we performed a virtual screening of our in-house database (27 905 compounds, National Center for Pharmaceutical Screening, Chinese Academy of Medical Sciences). The database was first filtered by the applicability domains of the two models, resulting in 20 912 compounds for NB-1-LPFP4 and 20 832 compounds for NB-2-LCFP6, respectively. For NB-1-LPFP4 model, eight probability outputs ( $P_{i+1}$  and  $P_{i-1}$   $i = 1, 2, 3, 4$ ) were predicted for each compound using four single classifiers (NN-c1, kNN-c1, CT-c1, and RF-c1). Together with LPFP4 fingerprint, each compound outputted the final two combination decision probabilities ( $P_{C+1}$  and  $P_{C-1}$ ) with NB-1-LPFP4. Out of the 20 912 compounds screened, 2494 compounds were predicted as neuroprotective compounds against glutamate-induced neurotoxicity. Similarly, for NB-2-LCFP6 model, 4341 compounds were obtained against H<sub>2</sub>O<sub>2</sub>-induced neurotoxicity. Interestingly, 1614 compounds were predicted active by the two models simultaneously, and 553 out of them got both of the final probabilities  $P_{C+1}$  higher than 0.5 and were chosen for further study.

In addition, 553 compounds were clustered into 20 groups by FCFP<sub>6</sub> fingerprint with the Cluster ligands module in Discovery studio 4.0. Clustering is based on the root-mean-square (RMS) difference of the Tanimoto distance for fingerprinting. For each cluster, scaffold novelty as well as probability output was considered. Finally, 70 compounds (Table S7†) were obtained from our in-house sample library for *in vitro* neuroprotective assay.

### 3.8 *In vitro* neuroprotective assay results

The preliminary neuroprotective assay results were given in Table S8.† Among 70 compounds screened at the concentration of 30 μM, 33 compounds showed the preliminary neuroprotective effects (cell damage inhibition higher than 40%) on monosodium glutamate-induced neurotoxicity on PC12 cell, while 28 out of these 33 compounds exhibited neuroprotective effects on H<sub>2</sub>O<sub>2</sub>-induced neurotoxicity. 40% compounds (28/70) showed neuroprotective activity against glutamate-induced and H<sub>2</sub>O<sub>2</sub>-induced neurotoxicity simultaneously, which suggested that the prediction models could greatly increase the chance of identifying neuroprotective compounds.

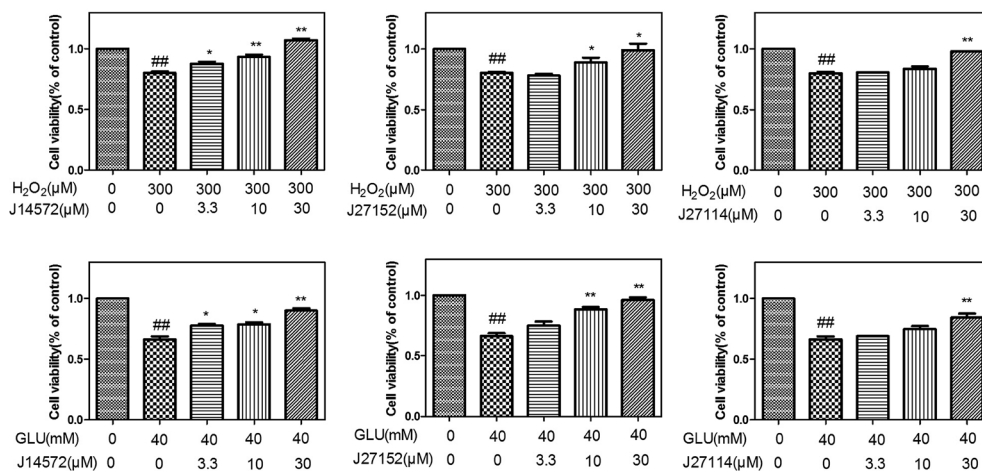


Fig. 8 Cytoprotective effects of chemicals on monosodium glutamate-induced and H<sub>2</sub>O<sub>2</sub>-induced PC12 cells. The viability of the untreated cells was set to 100%. The values represent mean (%) ± SEM of three individual experiments ( $n = 3$ ). # $P < 0.05$  and ## $P < 0.01$  versus control groups; \* $P < 0.05$  and \*\* $P < 0.01$  versus model group.

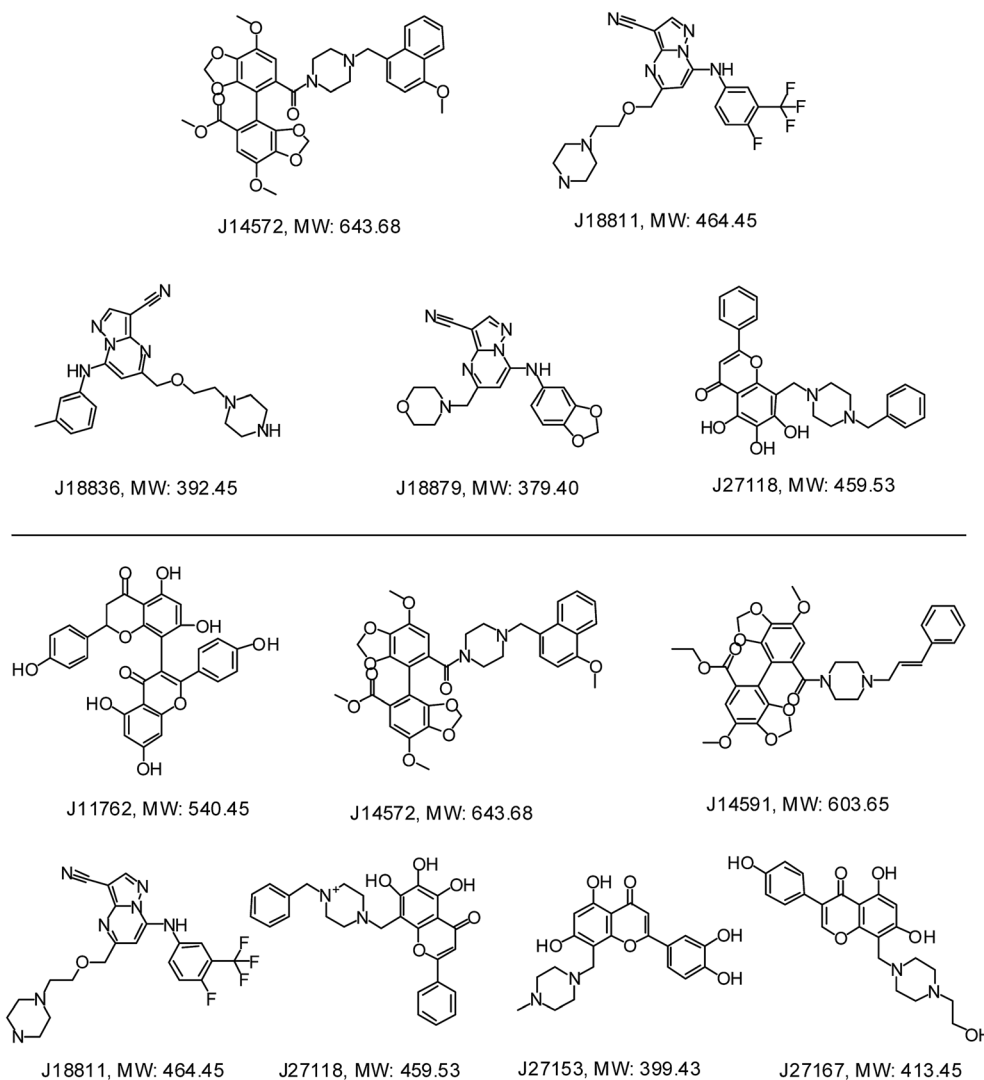


Fig. 9 Chemical structures of representative neuroprotective compounds against glutamate-induced (top) or H<sub>2</sub>O<sub>2</sub>-induced (bottom) neurotoxicity in PC12 cell.

Further evaluation results for the 28 compounds at different concentrations were given in Table 6. Vitamin E was set as reference compound and displayed neuroprotective effects.<sup>54</sup> Most of compounds exhibit good dose–response relationship, which means cell survival increases as the concentration of compound increases. Fig. 8 displays neuroprotective effects of three representative compounds (J14572, J27152 and J27114) on monosodium glutamate-induced and H<sub>2</sub>O<sub>2</sub>-induced PC12 cells. Compared with control group, cell survival for model group injured by 40 mM monosodium glutamate or 300 μM H<sub>2</sub>O<sub>2</sub> decreased significantly ( $P < 0.01$ ). After treatment with J14572 (3.3 μM, 10 μM and 30 μM), J27152 (10 μM and 30 μM) or J27114 (30 μM), cell survival increased significantly.

Further examination suggested five compounds (J14572, J18811, J18836, J18879 and J27118) could exhibited significant neuroprotective effects against monosodium glutamate-induced neurotoxicity at the concentration of 3.3 μM, 10 μM and 30 μM, while seven compounds (J11762, J14572, J14591, J18811, J27118, J27153 and J27167) displayed significant neuroprotective activity against H<sub>2</sub>O<sub>2</sub>-induced neurotoxicity at the same three concentration. The chemical structures of these potent compounds are shown in Fig. 9. To be exciting, three compounds (J14572, J18811, and J27118) could protect against glutamate-induced and H<sub>2</sub>O<sub>2</sub>-induced neurotoxicity at three concentrations, which showed promising prospect on neurodegenerative disease.

## 4. Conclusion

In this study, the classification models were developed to discriminate neuroprotective compounds against glutamate or H<sub>2</sub>O<sub>2</sub>-induced neurotoxicity from inactive through machine learning approaches. Twenty four single models were generated based on four different classification algorithms (neural network,  $k$  nearest neighbors, classification tree and random forest), which were integrated to develop the combined Bayesian models to obtain superior performance. The various validations including cross validation, test set validation, and Y-scrambling confirmed the prediction reliability of the models. Finally, two best models NB-1-LPFP4 and NB-2-LCFP6 were used to perform virtual screening for discovering neuroprotective compounds.

Preliminary assay results suggested that 40% (28/70) of compounds showed neuroprotective activity against glutamate-induced and H<sub>2</sub>O<sub>2</sub>-induced neurotoxicity simultaneously, and further evaluation showed that several of them could exhibit neuroprotective effects at different concentration (3.3 μM, 10 μM and 30 μM).

In short, this investigation demonstrated that *in silico* phenotypic-based models could efficiently identify novel neuroprotective compounds. This study provided useful suggestions for other types of rational drug discovery, and may be applied for other lead identification.

## Conflict of interest

The authors declare no competing financial interest.

## Acknowledgements

This work was funded in part of the Research Special Fund for the National Great Science and Technology Projects (2012ZX09301002-001-001), the International Collaboration Project (2011DFR31240), and Peking Union Medical College graduate student innovation fund (2013-1007-18).

## References

- 1 D. C. Rubinsztein, *Nature*, 2006, **443**, 780–786.
- 2 K. J. Barnham, C. L. Masters and A. I. Bush, *Nat. Rev. Drug Discovery*, 2004, **3**, 205–214.
- 3 B. Halliwell, *Drugs Aging*, 2001, **18**, 685–716.
- 4 C. Behl, J. B. Davis, R. Lesley and D. Schubert, *Cell*, 1994, **77**, 817–827.
- 5 H. Irannejad, M. Amini, F. Khodaghali, N. Ansari, S. K. Tusi, M. Sharifzadeh and A. Shafiee, *Bioorg. Med. Chem. Lett.*, 2010, **18**, 4224–4230.
- 6 E. K. Michaelis, *Prog. Neurobiol.*, 1998, **54**, 369–415.
- 7 L. Wang, Q. Gu, X. Zheng, J. Ye, Z. Liu, J. Li, X. Hu, A. Hagler and J. Xu, *J. Chem. Inf. Model.*, 2013, **53**, 2409–2422.
- 8 D. C. Swinney, *Clin. Pharmacol. Ther.*, 2013, **93**, 299–301.
- 9 W. Zheng, N. Thorne and J. C. McKew, *Drug Discovery Today*, 2013, **18**, 1067–1073.
- 10 J. Arrowsmith, *Nat. Rev. Drug Discovery*, 2011, **10**, 87.
- 11 D. C. Swinney and J. Anthony, *Nat. Rev. Drug Discovery*, 2011, **10**, 507–519.
- 12 J. T. Coyle and P. Puttfarcken, *Science*, 1993, **262**, 689–695.
- 13 Y. C. Kim, S. R. Kim, G. J. Markelonis and T. H. Oh, *J. Neurosci. Res.*, 1998, **53**, 426–432.
- 14 A. Vogt and J. S. Lazo, *Pharmacol. Ther.*, 2005, **107**, 212–221.
- 15 K. C. Peach, W. M. Bray, D. Winslow, P. F. Linington and R. G. Linington, *Mol. Biosyst.*, 2013, **9**, 1837–1848.
- 16 R. M. Pruss, *CNS Neurol. Disord.: Drug Targets*, 2010, **9**, 693–700.
- 17 R. Macarron, M. N. Banks, D. Bojanic, D. J. Burns, D. A. Cirovic, T. Garyantes, D. V. Green, R. P. Hertzberg, W. P. Janzen, J. W. Paslay, U. Schopfer and G. S. Sittampalam, *Nat. Rev. Drug Discovery*, 2011, **10**, 188–195.
- 18 S. Ananthan, E. R. Faaleolea, R. C. Goldman, J. V. Hobrath, C. D. Kwong, B. E. Laughon, J. A. Maddry, A. Mehta, L. Rasmussen, R. C. Reynolds, J. A. Secrist III, N. Shindo, D. N. Showe, M. I. Sosa, W. J. Suling and E. L. White, *Tuberculosis*, 2009, **89**, 334–353.
- 19 N. Singh, S. Chaudhury, R. Liu, M. D. M. AbdulHameed, G. Tawa and A. Wallqvist, *J. Chem. Inf. Model.*, 2012, **52**, 2559–2569.
- 20 F. Tomás-Vert, F. Perez-Gimenez, M. T. Salabert-Salvador, F. Garcia-March and J. Jaen-Oltra, *J. Mol. Struct.: THEOCHEM*, 2000, **504**, 249–259.
- 21 Y. Marrero-Ponce, R. Medina-Marrero, F. Torrens, Y. Martinez, V. Romero-Zaldivar and E. A. Castro, *Bioorg. Med. Chem.*, 2005, **13**, 2881–2899.
- 22 S. Ekins, R. C. Reynolds, S. G. Franzblau, B. Wan, J. S. Freundlich and B. A. Bunin, *PLoS One*, 2013, **8**, e63240.

- 23 E. L. Berg, J. Yang and M. A. Polokoff, *J. Biomol. Screening*, 2013, **18**, 1260–1269.
- 24 P. Prathipati, N. L. Ma and T. H. Keller, *J. Chem. Inf. Model.*, 2008, **48**, 2362–2370.
- 25 A. Gaulton, L. J. Bellis, A. P. Bento, J. Chambers, M. Davies, A. Hersey, Y. Light, S. McGlinchey, D. Michalovich, B. Al-Lazikani and J. P. Overington, *Nucleic Acids Res.*, 2012, **40**, D1100–D1107.
- 26 M. M. Mysinger, M. Carchia, J. J. Irwin and B. K. Shoichet, *J. Med. Chem.*, 2012, **55**, 6582–6594.
- 27 *Molecular Operating Environment (MOE), version 2010.10*, Chemical Computing Group Inc., Montreal, Quebec, Canada, 2010.
- 28 *Discovery Studio, version 4.0*, Accelrys Inc., San Diego, CA, 2013.
- 29 L. Wang, M. Wang, A. Yan and B. Dai, *Mol. Diversity*, 2013, **17**, 85–96.
- 30 M. Hall, E. Frank, G. Holmes, B. Pfahringer, P. Reutemann and I. H. Witten, *ACM SIGKDD explorations newsletter*, 2009, **11**, pp. 10–18.
- 31 D. E. Goldberg and J. H. Holland, *Mach. Learn.*, 1988, **3**, 95–99.
- 32 Version 2.7, available free of charge at Web site: <http://www.aillab.si/orange/>.
- 33 K. Gurney, *An introduction to neural networks*, CRC press, 1997.
- 34 D. T. Larose, *k-Nearest Neighbor Algorithm. Discovering Knowledge in Data: An Introduction to Data Mining*, 2005, pp. 90–106.
- 35 J. R. Quinlan, *C4. 5: programs for machine learning*, Morgan kaufmann, 1993, vol. 1.
- 36 L. Breiman, *Mach. Learn.*, 2001, **45**, 5–32.
- 37 J. C. Baber, W. A. Shirley, Y. Gao and M. Feher, *J. Chem. Inf. Model.*, 2006, **46**, 277–288.
- 38 N. Baurin, J.-C. Mozziconacci, E. Arnoult, P. Chavatte, C. Marot and L. Morin-Allory, *J. Chem. Inf. Comput. Sci.*, 2004, **44**, 276–285.
- 39 F. Cheng, Y. Yu, J. Shen, L. Yang, W. Li, G. Liu, P. W. Lee and Y. Tang, *J. Chem. Inf. Model.*, 2011, **51**, 996–1011.
- 40 J. R. Votano, M. Parham, L. H. Hall, L. B. Kier, S. Oloff, A. Tropsha, Q. Xie and W. Tong, *Mutagenesis*, 2004, **19**, 365–377.
- 41 J. Fang, R. Yang, L. Gao, S. Yang, X. Pang, C. Li, Y. He, A.-L. Liu and G.-H. Du, *Mol. Diversity*, 2015, **19**, 149–162.
- 42 X. Xia, E. G. Maliski, P. Gallant and D. Rogers, *J. Med. Chem.*, 2004, **47**, 4463–4470.
- 43 M. Luo, T. E. Reid and X. S. Wang, *Comb. Chem. High Throughput Screening*, 2015, **18**, 685–692.
- 44 J. Fang, R. Yang, L. Gao, D. Zhou, S. Yang, A.-L. Liu and G.-H. Du, *J. Chem. Inf. Model.*, 2013, **53**, 3009–3020.
- 45 J. Fang, Y. Li, R. Liu, X. Pang, C. Li, R. Yang, Y. He, W. Lian, A.-L. Liu and G.-H. Du, *J. Chem. Inf. Model.*, 2015, **55**, 149–164.
- 46 Y. Xia, J. Xing and T. Krukoff, *Neuroscience*, 2009, **162**, 292–306.
- 47 K. Dong, J.-X. Pu, H.-Y. Zhang, X. Du, X.-N. Li, J. Zou, J.-H. Yang, W. Zhao, X.-C. Tang and H.-D. Sun, *J. Nat. Prod.*, 2012, **75**, 249–256.
- 48 S. Ma and Y. Dai, *Briefings Bioinf.*, 2011, **12**, 714–722.
- 49 D. S. Wishart, C. Knox, A. C. Guo, S. Shrivastava, M. Hassanali, P. Stothard, Z. Chang and J. Woolsey, *Nucleic Acids Res.*, 2006, **34**, D668–D672.
- 50 R. W. Stanforth, E. Kolossov and B. Mirkin, *QSAR Comb. Sci.*, 2007, **26**, 837–844.
- 51 S. Dimitrov, G. Dimitrova, T. Pavlov, N. Dimitrova, G. Patlewicz, J. Niemela and O. Mekenyan, *J. Chem. Inf. Model.*, 2005, **45**, 839–849.
- 52 S. Weaver and M. P. Gleeson, *J. Mol. Graphics Modell.*, 2008, **26**, 1315–1326.
- 53 F. Sahigara, K. Mansouri, D. Ballabio, A. Mauri, V. Consonni and R. Todeschini, *Molecules*, 2012, **17**, 4791–4810.
- 54 B. J. Josey, E. S. Inks, X. Wen and C. J. Chou, *J. Med. Chem.*, 2013, **56**, 1007–1022.